Synthesis, Characterization, and Ionic Conductivity of Nanocomposites: Polyelectrolyte Systems

J. Cardoso,[1] R. Montiel,[1] O. Manero[2]

[1]*Departamento de Física, Universidad Autónoma Metropolitana, A.P. 55-534, México, D. F. 09340, Mexico*
[2]*Instituto de Investigaciones en Materiales, Universidad Nacional Autónoma de México, A.P. 70-360, México D. F. 04510, Mexico*

Received 1 September 2009; accepted 21 December 2009
DOI 10.1002/app.31994
Published online 18 August 2010 in Wiley Online Library (wileyonlinelibrary.com).

ABSTRACT: The synthesis, diffraction patterns, thermal stability, and ionic conductivity properties of methacrylate-type polymers are analyzed here to assess their feasibility as polymer electrolytes. From the parent polymer, poly (*N,N*-dimethylaminoethylmethacrylate), herein labeled PDMAEMA, a protonated derivative was used to prepare polymer/Montmorillonite nanocomposites with various clay contents (1, 3, and 5 wt %). AC spectroscopy provided the ionic conductivity data for the polymers and clay–polymer nanocomposites. Evidences of nanocomposite formation are shown using transmission electron microscopy and wide-angle X-ray diffraction. © 2010 Wiley Periodicals, Inc. J Appl Polym Sci 119: 1357–1365, 2011

Key words: nanocomposites; dielectric properties; ionic conductivity; nanostructure; polymer electrolytes

INTRODUCTION

The synthesis of polymer-based nanocomposites containing organoclays has received considerable attention recently.[1–3] Polymer nanocomposites are generally reinforced with low level loadings ($\leq$5 wt %) of inorganic silicate clays such as vermiculite, montmorillonite (MMT), smectite, and hectorite. Such composites comprise extremely thin, nanoscale dispersions of silicate platelets in a polymer matrix. Because of the nanoscale structure of the dispersion, nanocomposites possess unique mechanical, chemical, and thermal properties, excellent mechanical strength and stiffness, enhanced gas barrier behavior, good flame retardancy, and increased solvent resistance when compared to the pristine polymers. The compatibility between the polymer/clay interface and the type of clay used would affect the mechanical performances of the resulting nanocomposites.[4]

Incorporation of layered silicates into polymer matrices has been suggested for over 50 years.[5] One of the earliest systematic studies dates back to 1949, when Bower[6] described the absorption of DNA by MMT. During the 1950s Carter et al.[7] developed organoclays as reinforcement of latex-based elastomers and the patent: "clay complexes with conjugated unsaturated aliphatic compounds of four to five carbon atoms" was obtained by Hauser and Kollman.[8] Uskov,[9] in 1960, found that the softening point of poly(methyl methacrylate) obtained by polymerization of methyl methacrylate increased using MMT modified with octadecylammonium. In 1961, Blumstein[10] proposed to introduce a polymer in the clay structure, and in 1963, Greenland[11] studied the poly(vinyl alcohol)/MMT system to show that a polymer may be directly inserted in the clay in aqueous solution. The incorporation of organoclay into a thermoplastic polyolefin matrix was studied by Nahin and Backlund,[12] obtaining organoclay composites with strong solvent resistance and high tensile strength by irradiation-induced cross-linking. However, these preliminary studies did not analyze in detail the intercalation process in the clay and the potential properties of composites. In 1975, Tanihara and Nakagawa[13] analyzed the intercalation of polyacrylamide and polythylene oxide in aqueous solution, and in 1976, Fujiwara and Sakamoto[14] described the process to obtain the first organoclay hybrid polyamide nanocomposite. Later, the Toyota research group disclosed improved methods to obtain Nylon-6 clay nanocomposites using *in situ* polymerization methods, similar to the Unichika process. They reported that these polymer–clay nanocomposites exhibit superior strength, modulus, heat distortion temperature, water and gas barrier properties, with comparable impact strength as neat Nylon-6. They also reported that various types of

Correspondence to: J. Cardoso (jcam@xanum.uam.mx).
Contract grant sponsor: DCBI, UAM-I, and by the National Council for Science and Technology; contract grant number: CONACyT (CIAM2006/58646).

polymer–clay hybrid nanocomposites based on epoxy resins and polystyrene, acrylic polymer, rubber, and polyimides may be obtained using a similar approach. Moreover, work by Giannelis and coworkers[15,16] revealed that intercalation of polymer chains into the galleries of the organoclay can occur spontaneously by heating a mixture of the polymer and silicate clay powder in the melt. Once sufficient polymer mobility is achieved, chains diffuse into the host silicate clay galleries, thereby, producing an expanded polymer–silicate structure.

Although the intercalation chemistry of polymers when mixed with appropriately modified layered silicates and synthetic layered silicates has long been known, two major findings have stimulated a revival of the interest in polymer–layered silicate nanocomposite materials. The first one was the research on the Nylon-6/MMT nanocomposite in which very small amounts of layered silicate loadings resulted in significant improvements of thermal and mechanical properties; second, the observation by Giannelis and coworkers that it is possible to melt-mix polymers with layered silicates, without the use of organic solvents. Since then, the promise for important industrial applications has motivated vigorous research on a global scale, and efforts are focused on using almost all types of polymer matrices. In fact, nanocomposites have been proved with many thermoplastic and thermosetting polymers of different polarities, including polystyrene, polycaprolactone, polypropylene, poly(ethylene oxide), epoxy resin, polysiloxane, and polyurethane.[5,17–21]

The most commonly clay used in the synthesis of polymer nanocomposites is MMT, which is the major constituent of bentonite. It is well known that the filler anisotropy, that is, large length to diameter ratio (aspect ratio), is especially favorable in matrix reinforcement. Because of the unique structure of MMT, the mineral platelet thickness is only one nanometer, although its dimensions in length and width can be measured in hundreds of nanometers, with most of platelets lie in the 200–400 nm range after purification. Because of the characteristic size and thickness of the platelets, a single gram of clay contains over a million individual platelets.[22]

Two terms (intercalated and delaminated) are used to describe the two general classes of nanomorphology that can be prepared.[23] Intercalated structures are self-assembled, well-ordered multilayered structures where the extended polymer chains are inserted into the gallery space between parallel individual silicate layers separated by 2–3 nm. The delaminated (or exfoliated) structures result when the individual silicate layers are no longer close enough to interact with the adjacent gallery layers.[24] In the delaminated cases, the interlayer spacing can be on the order of the radius of gyration of the polymer; therefore, the silicate layers may be considered to be well-dispersed in the organic polymer. The silicate layers in a delaminated structure may not be as well-ordered as in an intercalated structure. Both of these hybrid structures can also coexist in the polymer matrix; this mixed nanomorphology is very common for composites based on smectite silicates and clay minerals, (For definitions and background on layered silicate and clay minerals see Ref. 25). Wide-angle X-ray diffraction (WAXD) measurements can be used to characterize these nanostructures if diffraction peaks are observed in the low-angle region: such peaks reveal the *d*-spacing (basal spacing) of ordered-intercalated and ordered-delaminated nanocomposites. However, if the nanocomposites are disordered, no peaks are observed in the X-ray patterns, due to loss of the structural patterns of the layers, the large *d* spacings (>10 nm), or both. Thus, WAXD of nanocomposites has limitations because a disordered, layered silicate can either be delaminated or intercalated. In such cases, transmission electron microscopy (TEM) combined with X-ray analysis characterize these materials more accurately.

Ion-conducting polymers (or polymer electrolytes) are materials that have attracted considerable attention for their vast applications in the development of solid-state ionic devices. Requirements such as high ionic conductivity, wide electrochemical stability windows, easy processability, and light-weight should be met, but in addition, acceptable thermal and mechanical performances are needed.[26] Intercalating polymers in layered clay-hosts render polymer electrolyte composites with huge interfacial area. Recently, the intercalation of modified clay in a polyethylene oxide (PEO) matrix in the melt has been reported.[27–30] The relationship among the thermal, electrical, and mechanical properties of this composite polymer-electrolyte was investigated by Nan and coworkers.[27] Such clay/PEO composites have high conductivity and high cation transference, and they can be produced into flexible films by adding a small amount of MMT to the PEO-based electrolyte. The ionic conductivity of these polymer electrolytes may be enhanced several decades more than the reference system conductivity.

In this article, the synthesis, characterization, and conductivity properties of methacrylate-type polymers are reported. The parent polymer is used to prepare three different nanocomposites. The thermal and ionic conductivity properties of the pristine polymer and nanocomposites are analyzed, with particular attention given to the relationship between ionic conductivity properties and nanostructure. Ionic conductivity data are provided by AC spectroscopy, which is the technique best suited to study amorphous conducting phases.[31] Data

analysis are carried out considering the frequency and temperature dependence of the dielectric parameters. This study provides new evidence concerning the influence of molecular structure on conductivity in nanocomposite systems.

MATERIALS AND EXPERIMENTAL PROCEDURE

Sample preparation–polymer preparation

N,N-Dimethylaminoethylmethacrylate (DMAEMA) was purified by vacuum distillation (84°C/15 mmHg). Bulk polymerization was carried out at 70°C for 20 h. 2,2′-Azobisisobutyronitrile (AIBN) was used as radical initiator. The yield of the reaction is 92%. The resulting polymer (herein labeled PDMAEMA) was dissolved in benzene, precipitated in cold hexane, dried in a vacuum oven at 50°C for 24 h and stored in a desiccator [see Fig. 1(A)]. PDMAEMA is an amorphous powder characterized by 1H-NMR ($CDCl_3$, 500MHz); δ (ppm) 0.9 and 1.1 (3H, 2s, —CH_3), 1.8, 1.9, 2.0 (2H, 3s, —CH_2—C(CH_3), 2.3 (6H, s, $(CH_3)_2$—N), 2.6 (2H, s, —CH_2—N); 4.1 (2H, t, CH_2—O); FTIR ($CHCl_3$) ν_{max} (cm^{-1}) 2960 (CH_3—, υ_{as}), 2926 (CH_2, υ_{as}), 1720 (C=O, υ_{st}), 1456 (CH_3—, δ_{as}).), 1100 (C—O—C). Analysis: C 59.97 %, H 9.60 %, N 8.83% calculated for repetitive unit: $C_8H_{15}NO_2 \cdot 2H_2O$, C 59.70 %, H 9.50 %, N 8.69%. $\langle M_w \rangle$ (CH_3OH) is 6.28×10^4 Da.

PDMAEMA was dissolved in a 1.0*M* HCl solution in 1 : 1 molar ratio at room temperature with overnight agitation. The protonated polymer (herein labeled PDMAEMAH=P) was precipitated in ethanol and washed with distilled water to obtain the purified salt [see Fig. 1(B)]. PDMAEMAH was also an amorphous powder characterized by FTIR. Thin films were prepared by the solution-casting method using trifluoroethanol as solvent. ^{1}H-NMR spectrum was carried out in D_2O. Analysis Elemental shows the following results: C 48.10%, H 9.38%, N 6.54% calculated for repetitive unit: $C_8H_{16}NO_2 \cdot 2.1\ H_2O$ C 49.28%, H 9.29 %, N 7.18%.

Organo-MMT preparation

MMT has ionic-interchange capacity of 135 meq/100g (Aldrich). Na-MMT is hydrophilic and not compatible with most organic molecules. The sodium cation in the interlayer spacing of MMT can be exchanged with organic cations to yield organophilic MMT (organo-MMT). For this purpose, ammonium cations of tetradecylammonium chloride ($C_{14}NH_4^+$) or a sulfobetaine zwitterion, dodecyldimethyl (3-sulfo-propyl) ammonium hydroxide, inner salt, (C_{12}SB) were used as surfactants.

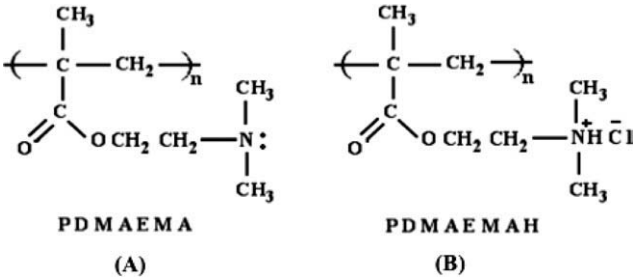

Figure 1 A: Chemical structure of the (PDMAEMA) polymer and B: protonated polymer (PDMAEMAH).

In a 1-L beaker, 24 mmol of the surfactant, 2.4 mL of concentrated hydrochloric acid, and 200 mL of water at 80°C were placed. The surfactant solution was added to a dispersion composed of 10 g of MMT and 1000 mL of hot water, and this mixture was stirred vigorously for 48 h giving a pink precipitate. The product was filtered, repeatedly washed with distilled water to remove the excess intercalant reagent, dried in a vacuum oven at 50°C for 48 h, and stored in a desiccator.

Nanocomposites preparation

Organo-MMT or MMT of 0.17 g alone was dispersed in 10 mL of distilled water, and then a solution composed of 3.17 g PDMAEMAH and 10 mL of distilled water was added slowly. The mixture was stirred for 48 h at room temperature under ultrasound to obtain homogenization (around 3 h). Under these conditions, C_{12}SB and PDMAEMAH behave as cationic surfactants. The obtained nanocomposites with 3% w/w composition were dried in a vacuum oven at 40°C and kept in a desiccator for further use. A similar procedure was followed for the other compositions. For dielectric measurements, films were obtained by casting, dissolving the nanocomposites in distilled water, and pouring them in cylindrical Teflon containers. They were left to evaporate slowly and placed them in a vacuum oven at 50°C until constant weight. The films so formed were transparent and kept in a desiccator.

Characterization of polymers and nanocomposites

Structure and molecular weight of the precursor polymer

FTIR spectra of the materials were recorded between 4000 and 400 cm^{-1} using a spectrometer (Perkin Elmer, USA). Thin films were prepared by the solution-casting method. A minimum of 32 scans were signal-averaged with a resolution of 2 cm^{-1}.

^{1}H-NMR spectra were carried out in a 5–10% weight solution of $CDCl_3$ with tetramethylsilane as

internal reference and deuterated water for precursor and protonated polymers, respectively, on a 500 MHz Brucker at room temperature. δ-units (ppm) were recorded. Elemental analysis was used to verify the chemical composition of the polymers, and light-scattering experiments were performed at room temperature in a Dawn-F (Wyatt Tech.) apparatus at $\lambda = 6320$ Å in methanol. The refractive index increment dn/dc was calculated (0.157 mL/g) in the same solvent at the same wave-length. Thermal properties were measured using differential scanning calorimetry (DSC) and thermogravimetry in a TA–DSC–TGA linked to a Thermal Analyzer 2100 microprocessor at a heating rate of 10°C/min under 50 mL/min nitrogen within the range of −50 to 500°C.

X-ray measurements

X-ray diffraction patterns for the nanocomposites were obtained in a diffractometer using Cu, K_α, α radiation, by performing sweeps from 2° to 70° of 2θ, at 1°/min.

Dielectric measurements

These measurements require that shape of the polymers remains unaltered throughout the experiment. For this purpose, a parallel-plate device with 20-mm diameter was used. Previously prepared solvent-cast nanocomposite slides of known thickness were placed in the holder of a Dielectric Analyzer (DEA, TA-Instruments). This device allows for a continuous contact between electrodes and sample. Ionic conductivity measurements were made from 30 to 80°C using a predetermined program. A nitrogen flux of 500 mL/min and an applied voltage of 1 V were used, within a frequency range from 1 Hz to 100 kHz.

High-resolution transmission electron microscopy measurements

Dried powder samples were placed in carbon and Formvar-coated Cu grids of 300 mesh size. Direct observation of the nanocomposite structures was carried out under bright field. The contrast between the dispersed clays and polymer matrix was sufficient for imaging without staining. High-resolution transmission electron microscopy (FEI Co., Tacnai T20 model, operated at 200 kV using a LaB6 filament) was used to assess the dispersion of the clay layers and tactoids in the nanocomposite films.

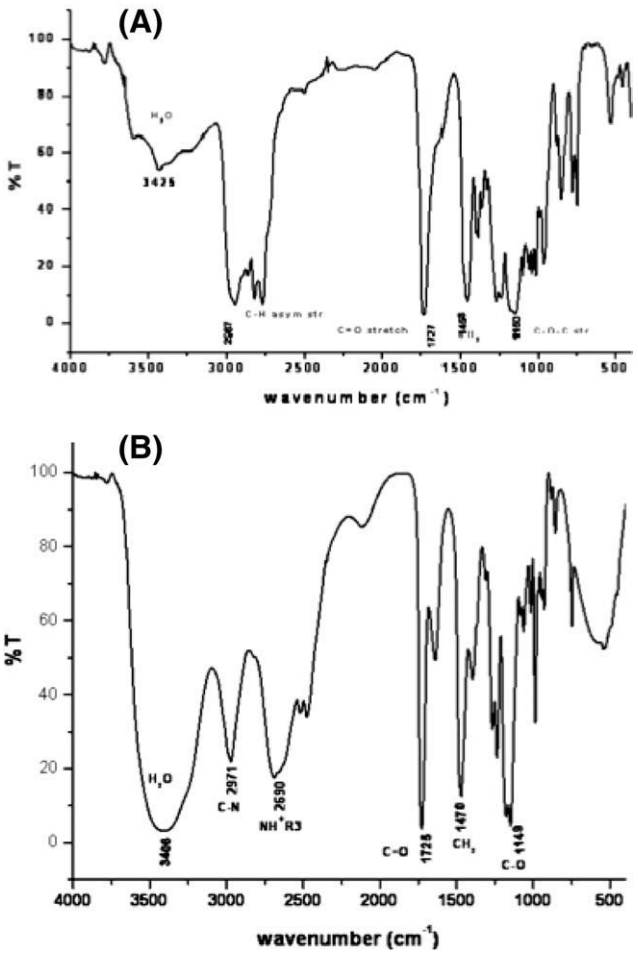

Figure 2 FTIR spectra of (A) precursor polymer and (B) protonated polymer.

RESULTS AND DISCUSSION

Chemical characterization of precursor and protonated polymer

PDMAEMA and PDMAEMH structures (Fig. 1) were verified by FTIR and ^{1}H-NMR spectra. Figure 2 shows the FTIR spectra of precursor (A) and protonated polymers (B). The main bands are described in the experimental part. Both PDMAEMH and PDMAEMA show a broad band around 3400 cm^{-1} and 1660 assigned to hydrates, showing the hydrogen bonding present in ammonium compounds, together with a strong band at 2640 cm^{-1} characteristic of the tertiary ammonium salt due to the vibration of N^+HR3 group, according to Ref. 32.

Figure 3 shows the ^{1}H-NMR spectra of the precursor [Fig. 3(A)], and protonated polymer [Fig. 3(B)]. The interpretation was described in the experimental part. The proton linked to the ammonium group (**N^+–H**) interchanges quickly with the deuterated water (**D_2O**), and therefore, the signal does not appear in the spectrum. In addition, it is observed that in contrast with the precursor polymer, all

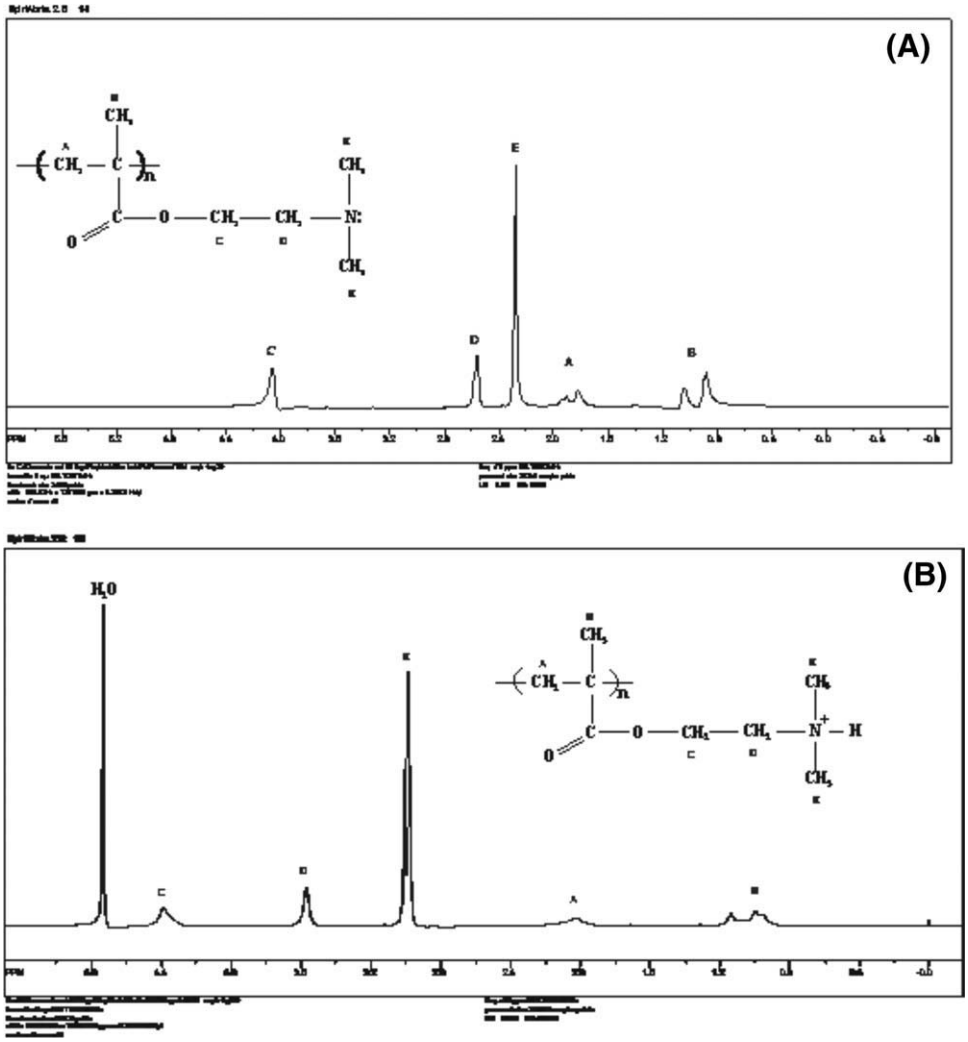

Figure 3 ^{1}H-NMR spectra of (A) precursor polymer and (B) protonated polymers.

bands in the protonated polymer are shift downfield due to the effect of the chemical modification. These data confirm the proposed chemical structure.

Thermal properties

DSC and thermogravimetric analysis (TGA) determined the glass transition temperatures (T_g) and thermal stability of polymers and nanocomposites. For both polymers and nanocomposites, T_gs were obtained from the second DSC-sweep as disclosed in Table I. T_g of the protonated polymer (PDMAEMAH) is 171°C, in contrast to 70°C for the same polymer synthesized by thermal initiation as reported by Chetia et al.[33] Explanation of this discrepancy may be due to the different molecular weights of the protonated polymer (6.24×10^4 Da) and the higher proton concentration used in this work. Polymer/3% PMMT/$C_{14}NH_4^+$ exhibits the highest T_g among the nanocomposites, attributed to the type of morphology (see later). In view of the very low organo-MMT loading, increases in T_g in the range of 2–20°C are measured.

The issue regarding the changes in T_g of polymer–clay nanocomposites is still controversial in the literature. Xu et al.[34] studied the epoxy/organo-MMT nanocomposites with diethylenetriamine. They

TABLE I
Thermal Properties of Precursor and Protonated Polymers and Nanocomposites

Sample	% MMT	% H_2O	T_g (°C)	$Td_{10\%}$ (°C)
MMT/$C_{14}NH_4^+$	–	1	–	136
PDMAEMA	–	16	32	173
PDMAEMAH = P	–	15	171	224
P/MMT/$C_{14}NH_4^+$	1	14	163	231
PMMT/$C_{14}NH_4^+$	3	13	168	234
P/MMT/$C_{14}NH_4^+$	5	15	160	228
P/MMT/C_{12}SB	1	14	162	281
P/MMT/C_{12}SB	3	10	158	285
P/MMT/C_{12}SB	5	12	157	267
P/MMT	3	13	151	210

TABLE II
Ionic Conductivity Properties of Protonated Polymer and Their Nanocomposites at 100 KHz as a Function of Temperature

Sample	% MT	Ionic Conductivity at 100 kHz			
		35°C	50°C	60°C	80°C
PDMAEMAH = P	–	1×10^{-9}	1.7×10^{-9}	1.6×10^{-9}	1.6×10^{-9}
P/MMT/$C_{14}NH_4^+$	1	1.6×10^{-6}	7.8×10^{-7}	4.4×10^{-7}	2.1×10^{-8}
PMMT/$C_{14}NH_4^+$	3	3×10^{-6}	8×10^{-6}	1.1×10^{-5}	1.6×10^{-5}
P/MMT/$C_{14}NH_4^+$	5	3.7×10^{-7}	2.1×10^{-7}	8.6×10^{-8}	2.6×10^{-8}
P/MMT/C_{12}SB	1	2×10^{-7}	2×10^{-7}	7×10^{-8}	1×10^{-8}
P/MMT/C_{12}SB	3	6×10^{-10}	2×10^{-9}	2×10^{-9}	$9 \times 10-^{10}$
P/MMT/C_{12}SB[a]	5	5×10^{-9}	6×10^{-9}	$4 \times 10-^{9}$	1×10^{-9}
P/MMT[a]	3	1×10^{-6}	$9 \times 10-^{5}$	2×10^{-4}	2×10^{-4}

[a] Obtained at 10 kHz

reported that the nanocomposite with 3% of organo-MMT has a lower T_g compared to the parent resin, as measured by dynamic mechanical analysis. This was attributed to the extra-gallery-cured epoxy resin, as the T_g of the highly confined epoxy in the inter-galleries was beyond the testing temperature range. A study on the melt intercalation of polystyrene in layered silicates showed that the magnitude of the DSC trace diminished upon intercalation, suggesting that only the unintercalated polymer contributed to the measured glass transition trace.[35]

Fan et al.[27] showed that when modified MMT is added to $(PEO)_{16}$ $LiClO_4$-based composite polymer electrolytes, a reduction in the T_g is obtained. As T_g lowers, the amorphous phase becomes more flexible; hence the ionic conductivity should be enhanced at low temperatures.

The observed increase of T_g in the nanocomposites obtained in this work may be associated to two causes: first, as the silicate layers interact with the polymer matrix through the ionic groups, the segment motion of the extragallery polymer is still affected by the unintercalated and exfoliated silicate layers, and then the interaction among ionic groups increases the T_g. This interpretation is in close agreement with Guo et al.[36] Samples with higher organo-MMT loading exhibited a moderate decrease in T_g. This may be due to increased aggregation of organo-MMT in the composite as the amount of organo-MMT increases and, therefore, this leads to an increase in the flexibility of the chain.[27]

The interactions of the intercalated chains of the polymer with the host species greatly reduce their rotational and translational mobility. The situation is similar to that in a reticulated polymer, where restrictions on its mobility increase its glass transition temperature.

TGA data of the samples are shown in Table I. Percent humidity (%H_2O) and the decomposition temperatures at 10% weight losses ($Td_{10\%}$) for each sample are reported. TGA data reveal that samples are highly hygroscopic; however, there is a clear influence of the nanoclay on the material hygroscopic properties. The percentage of humidity for the precursor polymer was 16%, but this was reduced with the addition of clay. $Td_{10\%}$ for the polymers and these nanocomposites ranged from 210 to 285°C. Results show that the sulfobetaine surfactant significantly enhances the thermal stability of the nanocomposites, in contrast to the ammonia surfactant. Thermally stable polymers are sought for applications as polymer electrolytes; in this regard, P/organo-MMT shows the highest degradation temperature (267–285 °C) when C_{12}SB is used as surfactant.

Ionic conductivity properties

The ac-conductivities at different temperatures of the pristine polymer, protonated polymer, and nanocomposites with various modified-MMT contents are shown in Table II. Conductivity increases with increasing frequency, and so in Table II, conductivity values at 100 kHz are only listed. A drastic two-decade increase in conductivity of PDMAEMA with the addition of 1 and 5 wt % clay using $C_{14}NH_4^+$ as surfactant is revealed. The highest value is 9.6×10^{-7} S/cm at 35°C. The decrease in T_g of PDMAEMA/1% (C_{12}SB-MMT) is ascribed to an increase in the segmental motion of the polymer, enhancing the conductivity (2.7×10^{-7} S/cm) at temperatures below the glass transition. These results indicate that the MMT-polymer electrolyte interface effect is not very important for ionic conduction. Kurian et al.[37] provide evidences for single-ion conduction in polymer–silicate nanocomposite electrolytes and confirmed that the conductivity arises from ionic motion. Likewise, in the nanocomposites analyzed here, two different ions Na^+ from MMT and H^+ from $C_{14}NH_4^+$ and PDMAEMAH are present, and therefore, the conductivity may be caused by these ion motions.

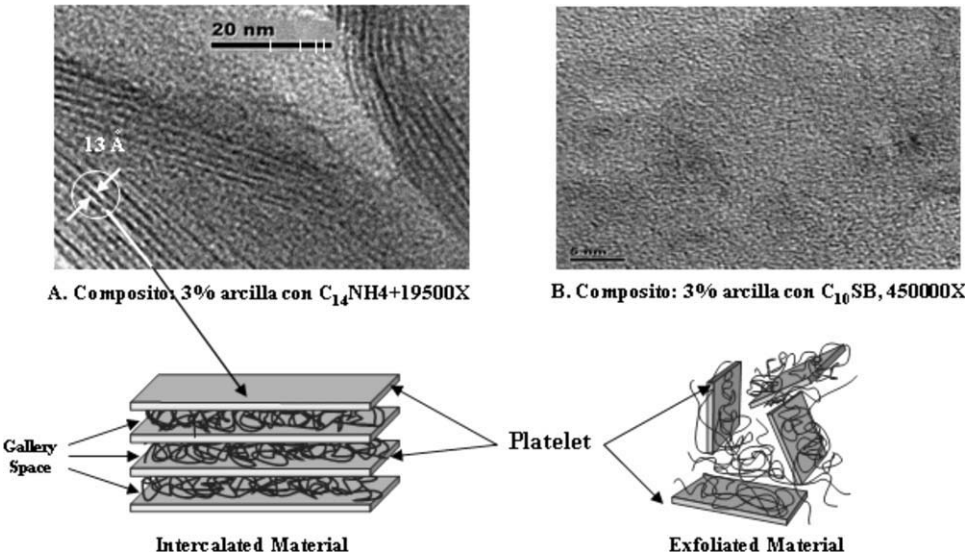

Figure 4 TEM images of (A) PDMAEMAH/3% $C_{14}NH_4$-MMT, (B) DMAEMA/3% $C_{12}SB$-MMT nanocomposites, and schematic model of the MMT structure, showing the intercalation of polymer molecules in the silicate platelets.

It is interesting to mention that in PDMAEMA/3% MMT or in 3% $C_{14}NH_4^+$-MMT samples the conductivity increases monotonically; however, the behavior is not Arrhenius like. The highest ionic conductivities values for these samples were 2×10^{-4} S/cm and 1.6×10^{-5} S/cm respectively, at 80°C. It has been suggested that the formation of percolating trajectories via polymer–inorganic interfaces may be important for ionic conduction.[27,38] Present results may rule out this assumption, since in the composites T_g increases as the polymer intercalates in the MMT galleries as shown in the morphology of the P/3% organoclay systems. The increase in the ionic conductivity at low temperature and its decrease at high temperatures make the composite polymer electrolyte less dependent on temperature, which makes it more suitable for applications.[27] Conductivities between 10^{-4} and 10^{-5} S/cm have been reported for [clay/PEO] nanocomposites (70–75 wt % clay at 250°C),[21] whereas other [clay/polymer] systems[39,40] exhibited conductivities in the range of 10^{-8} to 10^{-10} S/cm (10 wt % in the range of 85–110°C). Although the highest conductivity values reported here are low in comparison with other polymer electrolytes, the systems described in this work are salt free. Further work is needed to assess the suitability of these systems focusing on the development of oriented morphologies.

Nanomorphologies

Recent alternatives to produce polymer electrolytes with improved properties include polymer clay nanocomposites using various polymeric matrices. Clays used for preparation of nanostructures belong to the smectite group, and MMT is most commonly used. The crystal structure of the smectite group consists of a two-dimensional, 1-nm thick layers of two tetrahedral sheets of silica fused to an edge-shaped octahedral sheet of alumina where the octahedral site is isomorphically substituted.[41]

Together with X-ray analyses (WAXD), TEM results further support the occurrence of blend composites at the nanoscale level. The basal spacing d (001) from X-ray diffraction measurements is calculated at peak positions according to Bragg's law, $d = \lambda/(2 \sin \theta)$, where θ is the diffraction angle. The X-ray diffractograms of polymer–clays give a shift in the position of [001] planes (2θ changed from 7.2° to 3.3°), revealing increases in the basal spacing of these planes. The increase was relatively large, from 1.2 to 2.6 nm, and confirms the occurrence of polymer molecule intercalation between silicate platelets (indication of increasing of the interlayer spacing of clay layers, see Ref 42). These observations indicate that the main effect of the organic modifier in layered silicates is the intercalation in [001] planes of MMT. The basal spacing of layered silicates depends on the polymer modifier, increasing with concentration of the modifier. In this work, using two modifiers with the same organo-MMT concentration, different nanocomposite morphologies were obtained. Figure 4(A) shows high-resolution TEM images for two nanocomposites with P/3% organo-MMT with $C_{14}NH_4^+$or $C_{12}SB$ as surfactants. In image A, layers or clay laminates (bright lines) are observed. The basal spacing d (001) can be measured directly in the tactoid images, lying perpendicular to the beam, giving an average value of d (001) ≈13 Å, which is in good agreement to the value obtained by X-ray analysis, that is, d (001) ≈26 − 12 = 14 Å.

Figure 4(B) shows dispersed clay aggregates in the polymer matrix, oriented at random. When MMT concentration is high, uniform dispersion of clay in the PDMAEMA matrix is difficult to achieve, leading to the formation of phase-separated morphologies. This is expected to affect the conductivity of the systems, as the Na^+ (from MMT) carriers are no longer uniformly distributed throughout the material. Moreover, the clay platelets may be acting as physical barriers to the effective motion of carriers, thus leading to a decrease in conductivity of the ions below that of PDMAEMAH.

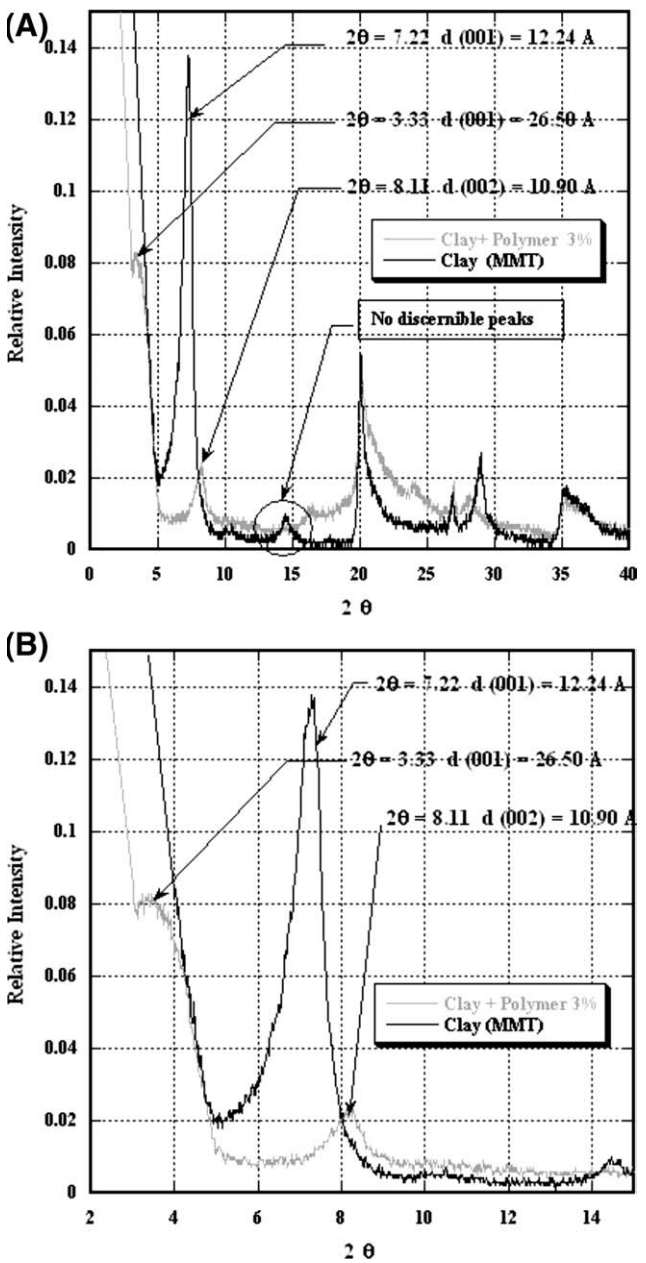

Figure 5 A: XR diffractogram of MMT and PDMAEMAH/3% -MMT and B: Magnification of the 2θ region, 2°–15°.

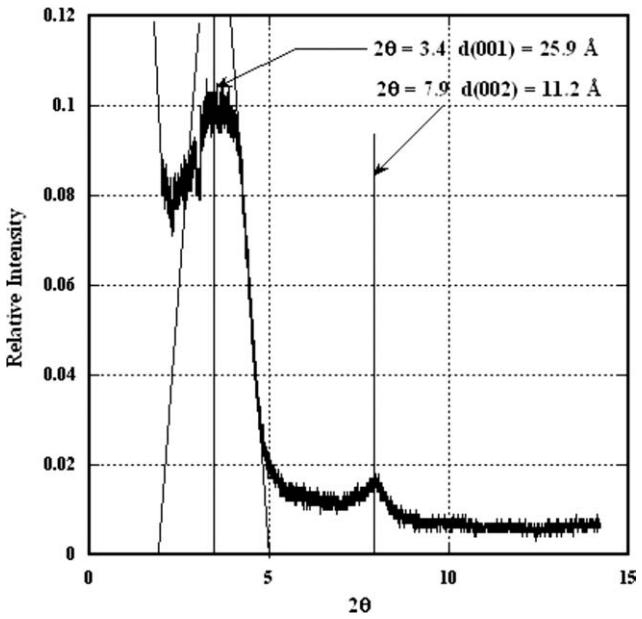

Figure 6 XR diffractogram of the PDMAEMA/1%C_{12}SB-MMT sample, showing a strongly inhomogeneous structure.

A broadening of one of the diffraction peaks (or no discernible peaks) was observed, notwithstanding, a MMT basal spacing of 12.2 Å appears, as shown in Figure 5(A). However, the broad diffraction peaks (decrease in the intensity of the basal reflections) show that the composite increases the disorder of the nterlayer material due to the random arrangement of the host molecules, and therefore, this is an indication of a strong structural disorder and inhomogeneous composition in the interlayer spacing of samples.[43] Such arrangement would allow for an expansion of the interlayer spacing, as in sample PDMAEMA/1% C_{12}SB-MMT. Similar observations have been recently reported in Ref. 26, for MMT intercalated with neutral polar dodecylamine in a molar ratio of 4 : 1, where a strongly inhomogeneous structure (very broad diffraction peak like that of Figure 6, for the sample PDMAEMA/1% C_{12}SB-MMT) is observed. This peak looks like an interstratified mixture of a wide-scale basal spacing of 26 Å. The same conclusion regarding the intensity of the peaks and morphology of nanocomposites has been reached (for more details see Ref 44).

CONCLUSIONS

PDMAEMAH/organo-MMT composites have been prepared by solution casting. WAXD patterns and TEM images reveal intercalation of the polymer in the clay galleries when the concentration is 3% ($C_{14}NH_4^+$-MMT or MMT). By addition of modified MMT into the PDMAEMAH matrix, the ionic conductivity of the composite polymer electrolyte

increases with ionic content. The behavior of the ionic conductivity and thermal properties can be attributed to the interactions and morphology features of the MMTs in the polymer matrix. One aspect of this study deserves further attention. The properties of the intercalated nanocomposites here prepared suggest that the laminate structure imposes a strong anisotropy on the conductivity properties and this is exclusively of the cationic type. This result itself not only sheds light on the understanding of ionic transport in the confined spaces of galleries but also has innovative technological implications in the production of new solid electrolytes.

The authors wish to thank Dr V. Garibay of the Mexican Petroleum Institute, P. Castillo and J. Rocha for their technical advise, and to the facilities provided in UAM-I.

References

1. Zeng, Q. H.; Wang, D. Z.; Yu, A. B.; Lu, G. Q. Nanotechnology 2002, 13, 549.
2. Yoonessi, M.; Toghiani, H.; Daulton, T.; Lin, J.; Pittman, U. Macromolecules 2005, 38, 818.
3. Manias, E.; Touny, A.; Wu, L.; Strawhecker, K.; Lu, B.; Chung, T. C. Chem Mater 2001, 13, 3516.
4. Tjong, S. C.; Meng, Y. Z.; Hay, A. S. Chem Mater 2002, 14, 44.
5. Cho, J. W.; Paul, D. R. Polymer 2001, 42, 1083.
6. Bower, C. A. IOWA Agric Exp Station Res Bull 1949, 362, 39.
7. Carter, L. W.; Hendricks, J. G.; Bolley, D. S. U.S. Pat. 2,531,396 (1950).
8. Hauser, E. A.; Kollman, R. C. U.S. Pat. 2,951,087 (1960).
9. Uskov, I. A. Vysokomol Soed 1960, 2, 926.
10. Blumstein, A. Bull Chim Soc 1961, 899.
11. Greenland, D. J. J Colloid Sci 1963, 18, 647.
12. Nahin, P. G.; Backlund, P. S. U.S. Pat. 3,084,117 (1963).
13. Tanihara, K.; Nakagawa, M. Nippon Kagaku Kaishi 1975, 5, 782.
14. Fujiwara, S.; Sakamoto, T. Jpn Kokai Pat. 109,998 (1976).
15. Vaia, R. A.; Ishii, H.; Giannelis, E. P. Chem Mater 1993, 5, 1694.
16. Mehrotra, V.; Giannelis, E. P. Mater Res Soc Symp Proc 1990, 171, 39.
17. Lebaron, P. C.; Wang, Z.; Pinnavaia, T. J. Appl Clay Sci 1999, 15, 11.
18. Fornes, T. D.; Yoon, P. J.; Keskkula, H.; Paul, D. R. Polymer 2001, 42, 9929.
19. Manias E. Available at: http://raman.plmsc.psu.edu/~manias/ pdfs/nano2001b.pdf (accessed 2001).
20. Shelley, J. S.; Mather, P. T.; Devries, K. L. Polymer 2002, 42, 5849.
21. Chin, I.-J.; Thurn-Albrecht, T.; Kim, H.-C.; Russell, T. P.; Wang, J. Polymer 2001, 42, 5947.
22. Patel, H. A.; Somani, R. S.; Bajaj, H. C.; Jasra, R. V. Bull Mater Sci 2006, 29, 133.
23. Gilman, J. W.; Jackson, C. L.; Morgan, A. B.; Harris, R. Chem Mater 2000, 12, 1866.
24. Lan, T.; Pinnavaia, T. J Chem Mater 1994, 6, 2216.
25. Kroschurtz, J. S., Ed. Kirk- Othmer Encyclopedia of Chemical Technology, Vol. 6. John Wiley: New York, 4th ed., 1993.
26. Bruce, P. G. Solid State Electrochemistry; Cambridge University Press: Cambridge, 1995.
27. Fan, L.; Nan, C. W.; Li, M. Chem Phys Lett 2003, 369, 698.
28. Scrosati, B.; Croce, F.; Persi, L. J Electrochem Soc 2000, 5, 1718.
29. Croce, F.; Appetecchi, G. B.; Persi, L.; Scrosati, B. Nature 1998, 394, 456.
30. Appetecchi, G. B.; Croce, F.; Persi, L.; Ronci, F.; Scrosati, B. Electrochim Acta 2000, 45, 1481.
31. Mcdonald, J. R., Ed. Impedance Spectroscopy; John Wiley: New York, 1987.
32. Brissette, C.; Sandorfy, C. Can J Chem 1960, 38, 34.
33. Chetia, J. R.; Maullick, M.; Dutta., A.; Dass, N. N. Mat Sci Eng B 2004, 107, 134.
34. Xu, W. B.; Bao, S. P.; Nie, K. M.; He, P. S. Chin J Appl Chem 2000, 18, 469.
35. Sikka, M.; Cerini, L. N.; Ghosh, S. S.; Winey, K. I. J Polym Sci Part B: Polym Phys 1996, 34, 1443.
36. Guo, B.; Ouyang, X.; Cai, C.; Jia, D. J Polym Sci: Part B: Polym Phys 2004, 42, 1192.
37. Kurian, M.; Galvin, M. E.; Trapa, P. E.; Sadoway, D. R.; Mayes, A. M. Electrochim Acta 2005, 50, 2125.
38. Aranda, P.; Ruizhitzky, E. Chem Mat 1992, 4, 1395.
39. Przyluski, J.; Siekierski, M.; Wieczorek, W. Electrochim Acta 1995, 40, 2101.
40. Okamoto, M.; Morita, S.; Kotaka, T. Polymer 2001, 42, 2685.
41. Patel, H. A.; Somani, R. S.; Bajaj, H. C.; Jasra, R. V. Bull Mater Sci 2006, 29, 133.
42. Eslami, H.; Grmela, M.; Bousmina, M. J Polym Sci: Part B: Polym Phys 2009, 47, 1728.
43. Dubbin, W.; Goh, T.; Oscarson, D.; Hawthorne, F. Clays Clay Miner 1994, 42, 331.
44. Pospisil, M.; Kalendova, A.; Capkova, P.; Valaskova, M. J Colloid Interface Sci 2004, 277, 154.